Proc. Natl. Acad. Sci. USA
Vol. 90, pp. 8934–8938, October 1993
Biophysics

Structure of hydrated oligonucleotides studied by *in situ* scanning tunneling microscopy

T. W. JING*, A. M. JEFFREY†‡, J. A. DEROSE*, Y. L. LYUBCHENKO*§¶‖, L. S. SHLYAKHTENKO¶‖, R. E. HARRINGTON¶, E. APPELLA**, J. LARSEN*, A. VAUGHT*, D. REKESH*, F.-X. LU‡, AND S. M. LINDSAY*,††

Departments of *Physics and Astronomy, and §Microbiology, Arizona State University, Tempe, AZ 85287; †Department of Pharmacology and ‡Division of Environmental Sciences, College of Physicians and Surgeons, Columbia University, New York, NY 10032; ¶Department of Biochemistry, University of Nevada, Reno, NV 89557; and **Laboratory of Cell Biology, National Cancer Institute, National Institutes of Health, Bethesda, MD 20892

Communicated by Oscar L. Miller, Jr., July 2, 1993 (received for review March 18, 1993)

ABSTRACT **We have used the scanning tunneling microscope (STM) to image several synthetic oligonucleotides adsorbed onto a positively charged Au(111) electrode. The molecules were deposited and imaged in aqueous electrolyte under potential control, a procedure that eliminated the problem of the substrate artifacts that had limited some previous STM studies. Experiments were carried out with two types of single-stranded molecules (11 and 20 bases long) and three types of double-stranded molecules (20 and 61 base pairs and 31 bases with 25 bases paired and 6-base "sticky" ends). The molecules lie along symmetry directions on the reconstructed (23 × $\sqrt{3}$) gold surface, and length measurements indicate that they adopt simple base-stacked structures. The base stacking distances are, within experimental uncertainty, equal to the 0.33 nm measured for polymeric aggregates of stacked purines by direct imaging in identical conditions. The images show features consistent with helical structures. Double helices have a major-groove periodicity that is consistent with a 36° twist. The single helices appear to be more tightly twisted. A simple tunneling model of STM contrast generates good agreement between measured and calculated images.**

The scanning tunneling microscope (STM) can resolve atoms under water (1) and many images of biopolymers have been reported (2), including images of DNA which appear to show both the major and minor grooves of the double helix (3) and even atomic resolution (4). These images are controversial because they were obtained on graphite substrates, which can mimic DNA (5) even at the atomic scale (6). Dunlap *et al.* (7) have estimated the conductance of dry DNA in air by studying contiguous segments of metal-coated and bare molecules, concluding that dry DNA is too good an insulator to be imaged by STM. Allison *et al.* (8) have reported images of plasmid DNA chemically bound to gold and imaged in air. The images are reproducible, but the contrast is variable (it can change from negative to positive). An altogether different approach uses electrochemical methods to bind molecules onto a gold electrode, which is then imaged under a covering layer of electrolyte (9, 10). Reliability has been improved by maintaining potential control of the electrode during imaging (11). The deposition of molecules can be monitored with this process. Thus, in addition to imaging in an aqueous environment, the substrate artifacts that have plagued some other work can be ruled out. Despite these advantages, the full potential of the method was not realized owing to instrumental limitations (12). We have now built a new microscope and have used it to study a number of different oligomers. We have also verified our interpretation of images in a blinded experiment (A.M.J., T.W.J., J.A.D., A.V., D.R., F.-X.L., and S.M.L., unpublished work). We have now acquired considerable data on synthetic single- and double-stranded oligomers. These confirm the original interpretation of structure in STM images of DNA (10) and permit us to test a simple tunneling model of contrast. The quality of these images is such that there can be little doubt about the ability of the STM to form high-resolution images of DNA in water. We report some of this work here [fuller details will be provided elsewhere (13)].

EXPERIMENTAL PROCEDURES

Scanning Tunneling Microscopy. We have constructed a microscope with much-reduced drift (0.002 nm/s), a sample translation stage (±2 mm in the plane of scanning), and a hermetically sealed environmental chamber (sparged with humidified N_2 gas) and which operates at low set-point currents (as low as 1 pA in the electrolytes used in this work). It was operated by a commercial controller (NanoScope II from Digital Instruments, Santa Barbara, CA). Tips were etched from $Pt_{0.8}Ir_{0.2}$ and insulated in an automated version of the procedure described elsewhere (14). Substrates were Au(111) which was grown epitaxially on mica (15). They were stored under argon until used and show the 23 × $\sqrt{3}$ reconstruction [the surface structure observed in ultrahigh vacuum (16)] almost everywhere on the surface if scanned near the potential for zero charge (PZC) (17–19). The STM was calibrated by imaging gold atoms in the (111) surface. Calibration was checked before each run by measuring the spacing across the stacking faults associated with the 23 × $\sqrt{3}$ reconstruction (i.e., along [1$\bar{1}$0]; see Fig. 1*A*). Under water and at the rest potential, this spacing was usually within 0.25 nm of 6.75 nm (19). Height measurements were calibrated by using steps on the Au(111) surface (0.25 nm). The tunnel current set point (I_t), tip-to-substrate voltage (V_{TS}), and scanning speed (s) are listed in each figure caption. All images were obtained in the constant-current mode.

DNA Samples. We used the following oligonucleotides: An 11-base single-stranded (ss) DNA (sample 1), a 20-base ssDNA (sample 2); a 20-bp double-stranded (ds) DNA (sam-

The publication costs of this article were defrayed in part by page charge payment. This article must therefore be hereby marked "*advertisement*" in accordance with 18 U.S.C. §1734 solely to indicate this fact.

Abbreviations: C_B, buffer concentration; C_D, DNA concentration; H, height (contrast) of image; I_t, tunnel current; L, length; P, helical repeat; PZC, potential for zero charge; s, scanning speed; STM, scanning tunneling microscope; t_D, sample deposition time; V_{ED}, substrate potential for sample deposition; V_{EI}, substrate potential for imaging; V_{TS}, tip-to-substrate potential difference; W, width; ssDNA and dsDNA, single- and double-stranded DNA.

‖On leave from: Institute of Molecular Genetics, Russian Academy of Sciences, Moscow, Russia.
††To whom reprint requests should be addressed.

ple 3), a 31-bp dsDNA (with 6-base sticky ends; sample 4), and a 61-bp dsDNA (sample 5). Their sequences are listed below.

(1) 5′–GGCCCCCCGGG–3′

(2) 5′–GAAGAGAACCAAGAAGGAGA–3′

(3) 5′–TCTCCTTCTTGGTTCTCTTC–3′
3′–AGAGGAAGAACCAAGAGAAG–5′

(4) 5′–TGCTGATCTATCACCGCAAGGGATAAATATC–3′
3′–AGATAGTGGCGTTCCCTATTTATAGACGACT–5′

(5) 5′–TAATACGACTCACTATAGGCGACTGGTGAGTACGCCAAAAAT–
3′–ATTATGCTGAGTGATATCCGCTGACCACTCATGCGGTTTTTA–
TTTGACTAGCGGAGGCTAG–3′
AAACTGATCGCCTCCGATC–5′

Samples 1, 4, and 5 were synthesized with an Applied Biosystems model 392 DNA synthesizer and purified on a Waters model 510 HPLC system. Complementary strands were dissolved in SSC (0.15 M NaCl/0.015 M sodium citrate, pH 7), heated to 90°C, and cooled over a period of 1 hr. The samples were desalted on Sephadex G-50 columns and stored at −20°C until used. Samples 2 and 3 were synthesized with an Applied Biosystems 394 synthesizer, suspended in 0.1 M NaOH, and eluted from a prewashed Pharmacia NAP-5 column with TE (10 mM Tris·HCl/1 mM EDTA, pH 8.0). They were further purified on a Waters Gen-Pak Fax column with TE. Complementary single strands were annealed in TE at 60°C for 2 hr and cooled to room temperature over a period of 4 hr. DNA was repurified by HPLC and desalted by dialysis against deionized distilled water. Control samples were obtained from aliquots from the HPLC column that contained no DNA. Equimolarity of the strands was established spectroscopically (any remaining single-stranded material was removed by HPLC after annealing).

Solutions and Electrochemical Deposition. DNA was dissolved (0.1–30 μg/ml) in NaP_i (pH 7.0). EDTA was added in some runs. All buffers were made with 99.95% pure salts (Aldrich) and water from a Nanopure bioresearch-grade filtration system (Barnstead, Dubuque, IA). Specific buffer (C_B) and DNA (C_D) concentrations are listed in figure captions. The potential of the substrate was measured with a silver wire quasi reference. In these pH 7 buffers, 0 V on this electrode scale corresponds to 147 ± 10 mV on the saturated calomel electrode (SCE) scale. We quote potentials on the SCE scale. The substrate was first surveyed by STM imaging under solution with the counter electrode disconnected in order to establish its cleanliness. The STM tip was withdrawn a few micrometers, and the substrate potential was raised positive of the PZC and held for a time, t_D, at a potential V_{ED}. The tip was lowered and the substrate reimaged while held under potential control at a potential V_{EI}. Specific conditions are given in figure captions.

Image Analysis and Interpretation. Measurements of the length (L) and width (W) of images were made with the public-domain software NIH IMAGE 1.40. Height (H) was determined by using cross-section measurements made with the Nanoscope software and also by integrating image density over whole molecules and adjacent background using NIH IMAGE (with appropriate calibration of the gray scale). Measured standard deviations were combined with the calibration uncertainties (of 5%) to yield a final random error on the data. Large data sets (e.g., sample 1) displayed a correlation between L and W, presumably because of tip-induced broadening of both quantities, so some correction for tip broadening could be attempted (13). However, it was more useful to select those images that showed evidence of structure that was independent of tip geometry and analyze them with a detailed model (internal features were imaged in repeated runs to ensure that they were not a consequence of tip structure). Images are shown with no processing beyond leveling and contrast adjustment.

RESULTS AND DISCUSSION

Single-Stranded Oligomers. Our new microscope permits us to find the same area of the substrate after deposition of molecules, and Fig. 1 illustrates this with "before" (*A*) and "after" (*B*) scans. Prior to deposition, the peak-to-peak corrugation (Fig. 1*A*) was about 0.01 nm owing to some manifestation of the $23 \times \sqrt{3}$ reconstruction in the presence of phosphate buffer (12). The gold [11$\bar{2}$] and [1$\bar{1}$0] directions are indicated by arrows. After deposition, the corrugation in the same region (Fig. 1*B*) was about 0.2 nm. Many fragments of the single-stranded sample 2 were densely packed along the reconstruction with their long axes oriented in the [1$\bar{1}$0] direction (this was the preferred alignment for all the single-stranded polymers). Such features were not observed with control (no DNA) samples. This is illustrated in Fig. 1 *C* and *D*, where the peak-to-peak corrugation was about 0.03 nm. Results like these required that (*a*) the gold substrates were clean, showing the reconstructed surface over most of the surface, and (*b*) that the samples were not contaminated.

ssDNA is flexible and capable of hairpin formation and non-Watson–Crick base pairing (20). Its length need not be controlled by base stacking [but fiber diffraction suggests that

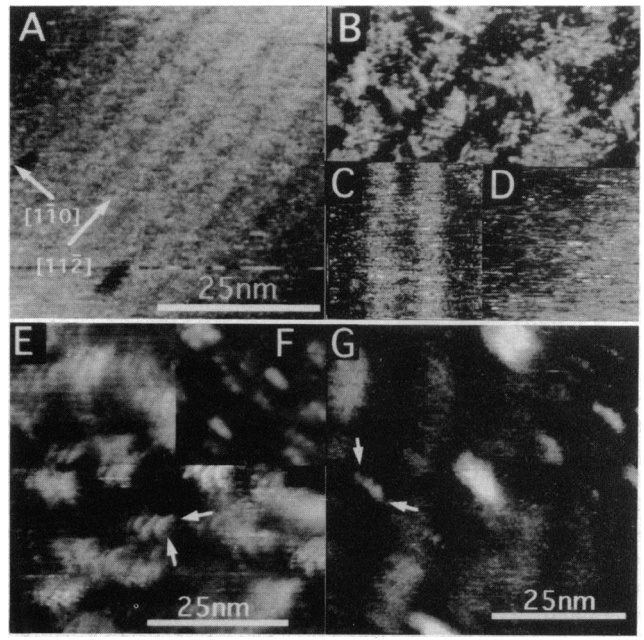

FIG. 1. Images of single-stranded oligomers. (*A* and *B*) Controlled deposition of DNA fragments on gold: Au(111) facet imaged under buffer containing DNA prior to deposition (*A*) and the same area after deposition of sample 2 (*B*). (*C* and *D*) Control experiments in which the deposition cycle was carried out with NaP_i (*C*) and NaP_i plus EDTA (*D*), but with no DNA present (magnification is the same for *A–D*). (*E* and *F*) Sample 1 (11 bases). (*G*) Sample 2 (20 bases). Arrows point to a single molecule. Conditions: (*A*) C_B = 2 mM NaP_i, C_D = 34 μg/ml (sample 2), I_t = 40 pA, V_t = −100 mV, s = 250 nm/s; (*B*) as in *A* with V_{ED} = 267 mV, t_D = 1 hr, V_{EI} = 267 mV; (*C*) C_B = 8 mM NaP_i, C_D = 0, V_{ED} = 267 mV, $t_D \approx$ 2 hr, I_t = 30 pA, V_{TS} = −100 mV, V_{EI} = 267 mV, s = 430 nm/s; (*D*) C_B = 4 mM NaP_i plus 0.25 mM EDTA, C_D = 0, V_{ED} = 267 mV, $t_D \approx$ 2 hr, I_t = 60 pA, V_{TS} = −100 mV, V_{EI} = 267 mV, s = 430 nm/s; (*E*) C_B = 1.6 mM NaP_i, C_D = 0.1 μg/ml (sample 1), V_{ED} = 247 mV, $t_D \approx$ 3 hr, I_t = 50 pA, V_{TS} = −100 mV, V_{EI} = 258 mV, s = 208 nm/s; (*F*) C_B = 1.6 mM NaP_i, C_D = 0.1 μg/ml, V_{ED} = 247 mV, t_D = 4 hr, I_t = 50 pA, V_{TS} = −100 mV, V_{EI} = 247 mV, s = 260 nm/s; (*G*) C_B = 5 mM NaP_i plus 5 μM EDTA, C_D = 3.2 μg/ml (sample 2), V_{ED} = 267 mV, t_D = 4 hr, I_t = 40 pA, V_{TS} = −100 mV, V_{EI} = 267 mV, s = 443 nm/s.

it may be (21)] and could conceivably vary from 0.2 to 0.6 nm per base (22). Therefore, one cannot rely upon the length of the images as the sole criterion for interpretation. Aggregation further complicates interpretation (13). However, comparison of images of sample 1 (Fig. 1 *E* and *F*) and sample 2 (Fig. 1*G*) shows that the images of the 20-base oligomer are about twice the length of the images of the 11-base oligomer, suggesting that both adopt the same extended (i.e., no hairpins) conformation. The contrast varies considerably from molecule to molecule (note the standard deviations of the measured heights listed in Table 1) so that images may be both faint or bleached-out in the same scan (Fig. 1*G*). Resolution can also vary from run-to-run; e.g., Fig. 1*F* shows resolution of internal structure in images of sample 1. We obtained length and width data for 105 well-separated molecules of sample 1 imaged in 12 separate runs. Similar data were compiled for 83 molecules of sample 2, imaged in 7 separate runs. Average values for L and W are given in Table 1. If we take the observed lengths and divide by the number of bases, we obtain an average rise per base (for the single-stranded samples) of 0.4 ± 0.08 nm. A better determination is obtained by considering only the longer oligomers, for which the rise per base is 0.35 ± 0.04 nm. This result is equal (within experimental error) to the value determined by direct imaging of polymeric aggregates of stacked purines obtained under identical conditions (23) and is close to the canonical value for B-DNA (22). Structural studies of single-stranded nucleic acids are limited in number but do suggest that such stacking occurs in normal conditions (21).

Images of sample 2 displayed an interesting dependence on packing density. Isolated molecules yielded images like those in Fig. 1*G*, where there is some evidence of three "blobs" along the image. Densely packed aggregates produced images like those in Fig. 1*B*, where there is a smaller distance between blobs. We refer to this as the 6-fold structure because the distance between blobs in the image is about half of that seen for the 3-fold (Fig. 1*G*) structure. Examples of both are shown in the second (2a) and third (2b) rows of Fig. 3. Data for the repeat distances (P) are listed in Table 1.

Double-Stranded Oligomers. Images of sample 3 (20-bp dsDNA) were usually broader than those of the ssDNA and appeared to be composed of two blobs separated by about 4 nm (essentially the pitch of B-DNA). The long axis of the molecules aligned along the [11$\bar{2}$] direction (this was the preferred orientation for all the double-stranded samples). Examples are shown in Fig. 2 *A–D*. Note that the resolution varies considerably from molecule to molecule. To verify that the blobs were due to turns of the double helix, we synthesized and imaged the 31- and 61-base dsDNAs, samples 4 and 5. Scans of all three samples are shown at about the same magnification in Fig. 2 *D–F*. They confirm that, broadly speaking, each blob is associated with a turn of the double helix: images of the 31-base sample (no. 4) show three blobs (Fig. 2*E*) whereas images of the 61-bp fragment (sample 5) show six blobs (Fig. 2*F*). Some smaller fragments are present in this image also.

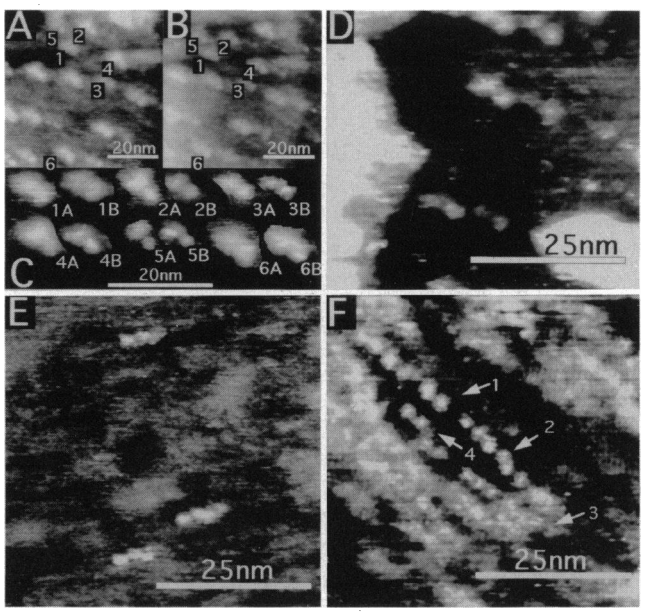

FIG. 2. Images of double-stranded oligomers. (*A* and *B*) Scans taken 3 min apart over the same adsorbate patch made with sample 3 (20 bp). (*C*) Individual molecules (labeled to lower left) are paired. (*D–F*) Scans of the same magnification for the 20-bp sample (*D*), the 31-base sample (*E*), and the 61-bp sample (*F*). In *F*, 1–3 are intact molecules. Arrow 4 points to fragments that may have been damaged by scanning. Conditions: (*A*) C_B = 5 mM NaP_i plus 5 μM EDTA, C_D = 4 μg/ml, V_{ED} = 267 mV, t_D = 2.5 hr, I_t = 30 pA, V_{TS} = −100 mV, V_{EI} = 267 mV, s = 623 nm/s; (*B*) as in *A* but with I_t = 50 pA and s = 333 nm/s; (*D*) C_B = 5 mM NaP_i plus 5 μM EDTA, C_D = 4 μg/ml, V_{ED} = 267 mV, t_D = 1.5 hr, I_t = 20 pA, V_{TS} = −100 mV, V_{EI} = 267 mV, s = 918 nm/s; (*E*) C_B = 5.5 mM NaP_i, C_D = 3.5 μg/ml, V_{ED} = 267 mV, t_D = 3 hr, I_t = 20 pA, V_{TS} = −100 mV, V_{EI} = 267 mV, s = 761 nm/s; (*F*) C_B = 5 mM NaP_i plus 5 μM EDTA, C_D = 24 μg/ml, V_{ED} = 267 mV, t_D = 1 hr, I_t = 20 pA, V_{TS} = −100 mV, V_{EI} = 267 mV, s = 717 nm/s.

The 20-bp duplex displays an unusually large molecule-to-molecule variation in width even within a given scan. This is illustrated in Fig. 2 *A* and *B*, two scans obtained 3 min apart after continuous scanning over the same area and adjustment of the microscope operating parameters (see caption). We have paired molecules in Fig. 2*C*, and it is clear the broadening is intrinsic to the molecules and cannot be accounted for by sample movement, tip geometry, or some other aspect of the microscope operation. It is possible that the variations are a consequence of contamination. On the other hand, the 31- and 61-base dsDNAs did not show similar variability, so that the width fluctuations in the shorter oligomer may reflect an intrinsic instability, possibly reflecting premelting fluctuations.

Table 1. Dimensions of STM images

Sample	n	L_{avg}, nm	W_{avg}, nm	P, nm	H, nm
(1) ss 11-mer	105	5.4 ± 1.0	2.0 ± 0.5	1.9 ± 0.3	0.11 ± 0.07
(2) ss 20-mer	44*	7.9 ± 0.9*	2.2 ± 0.5*	2.6 ± 0.6*	0.22 ± 0.07†
	39‡	6.2 ± 0.9‡	1.1 ± 0.3‡	1.3 ± 0.3‡	
(3) ds 20-mer	69	6.9 ± 0.8	3.2 ± 0.6	3.9 ± 0.5	0.21 ± 0.06
(4) ds 31-mer	18	8.8 ± 0.8	2.7 ± 0.3	3.0 ± 0.3	0.16 ± 0.11
(5) ds 61-mer	16	21.0 ± 2.1	2.9 ± 0.4	3.5 ± 0.6	0.19 ± 0.08

n, No. of molecules in sample; L_{avg}, length of image; W_{avg}, width of image; P, period of features along molecule (blob-to-blob distances); H, height of images.
*Data for 3-fold structure.
†Data from complete set of 83 molecules.
‡Data for 6-fold structure.

Values for the blob-to-blob distance listed for the three polymers (Table 1) fall within the normal range for the helix repeat of B-DNA structures (22). The estimated values of rise-per-base are 0.35 ± 0.03 nm for sample 3, 0.28 ± 0.03 nm for sample 4 if the sticky ends are imaged and 0.35 ± 0.03 nm if they are not, and 0.34 ± 0.03 nm for sample 5.

Comparison with Model Structures. Further analysis requires comparison with molecular models and this, in turn, requires a model for contrast (24–29). We have carried out many experiments in order to elucidate the mechanism of electron transport in the conditions in which we obtain DNA images (30). The main points are as follows.

(*i*) Barrier height and contrast measurements indicate that the electron transport mechanism is tunneling. Current-vs.-distance measurements imply barriers between 1.7 and 4 eV (depending upon the adsorbed species). For example, on clean gold, we obtain 2.1 ± 0.2 eV, in reasonable agreement with estimates of the tunnel barrier in a metal–liquid–metal junction (31, 32). Furthermore, measurements of the contrast as a function of the set-point tunnel current are consistent with a Tersoff–Hamann model of STM contrast using these measured values of barrier height (30, 34).

(*ii*) Few *ab initio* calculations of STM contrast for "insulating" atoms or molecules have been carried out. However, those that we are aware of show a remarkable phenomenon: the conducting states of the metal are propagated out into the vacuum by the atomic potentials as the metal wave functions orthogonalize to the atomic states (35, 36).

(*iii*) The question of whether or not an adlayer is insulating is more appropriately addressed by asking "at what point does the gap resistance become of order h/e^2?" (37, 38). This point (quantum point contact) is, at least approximately, independent of the local density of electronic states [because the current is the product of this density with the electron velocity, which is often the inverse of the density of states (38, 39)]. Therefore (in the spirit of these simple arguments) *any* residual density of metallic states will suffice to make a quantum point contact.

(*iv*) Cyclic voltammetry and capacitance measurements indicate that the DNA is buried in an adlayer of at least one (and perhaps three) hydrogen-phosphate molecules in depth (30). Adsorption is accompanied by a reversible electron transfer reaction.

(*v*) The key unknown parameter is the point at which the simple density-of-states arguments advanced in *iii* break down, so that any residual metallic density is unable to support quantum-point contact. Since the structure of the adlayer surrounding the DNA is unknown, we leave this

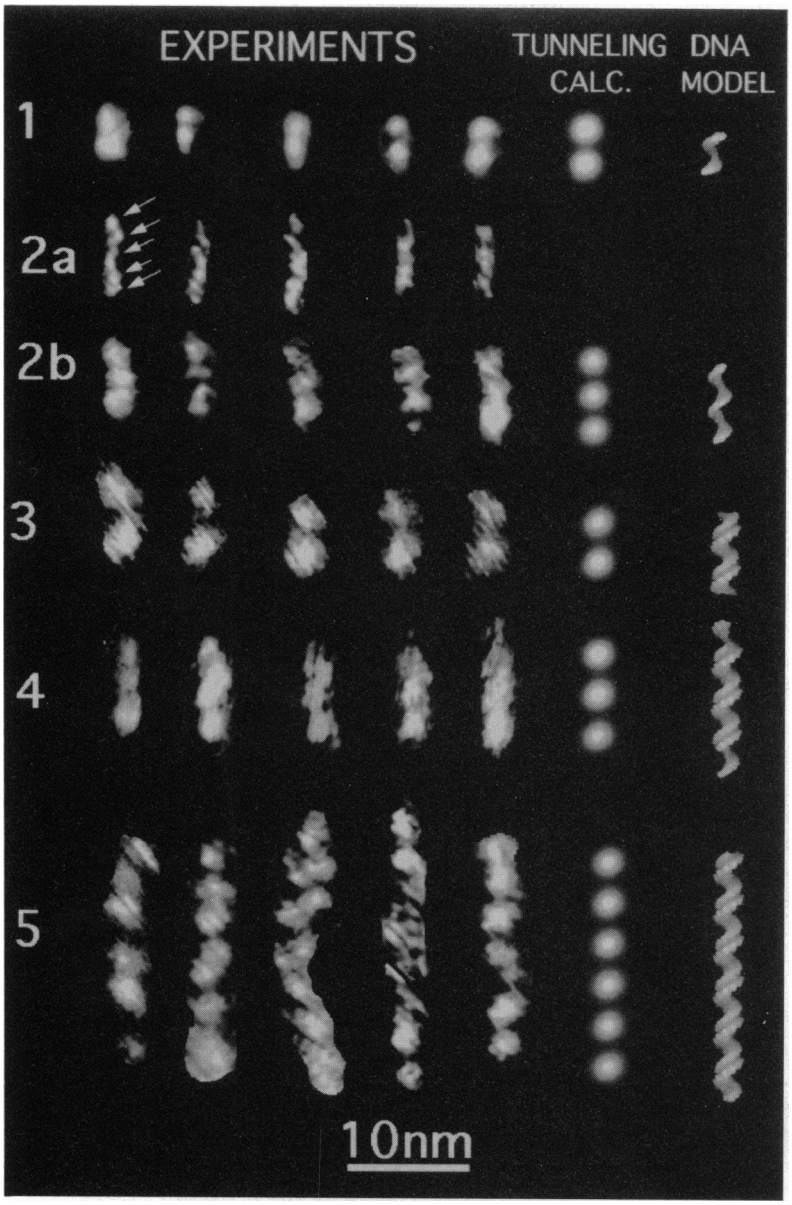

FIG. 3. Selection of five images from various runs for 1, the 11-base ssDNA; 2a, the "6-fold" 20-base ssDNA (arrows indicate periodicity); 2b, the "3-fold" 20-base ssDNA; 3, the 20-bp dsDNA; 4, the 31-base DNA with 25 paired bases; and 5, the 61-bp dsDNA. Structural models are shown to scale on the far right (see text). The calculated images (corresponding to these models) are shown next to the experimental data.

distance as an adjustable parameter. We assume that metallic states propagate out to the outermost atoms of the DNA, where they then decay at the rates we have measured (30).

(*vi*) The "tunnel gap" in these measurements is about 0.8 nm (as deduced from measured barriers). Therefore, the atomic details of the tip are not of overriding importance. Our tips are quite well described by parabolas of radii between 5 and 20 nm (14). This results in a Gaussian broadening of 0.6- to 1-nm radius (34).

(*vii*) The barrier heights over DNA molecules and the surrounding hydrogen-phosphate adlayer do not differ by a large factor (i.e., <2). Therefore the measured (small) image height (Table 1) of the DNA must reflect a small physical height: the DNA must be buried in a conducting (in the sense of quantum point contact) adlayer.

The simplest method for calculating images consistent with the above points is to (*a*) calculate the height of each point on a molecule above a substrate, (*b*) assume that only the uppermost 0.2 nm protrudes above the adjacent adlayer and calculate a gray-scale image in which gray level is linearly related to this difference in height (for the constant-current mode and ignoring atom-to-atom differences in decay constants), and (*c*) account for the tip shape with a Gaussian blurring of 0.6- to 1.0-nm radius.

This model permits the contrast of the STM image to be calculated if the azimuthal orientation of the molecule is known. Rhodes and Klug (33) have determined the preferred orientations of DNA molecules on charged substrates by an ingenious enzyme-digestion procedure. The two allowed orientations are those that equalize the interactions between the ends of the molecule and the substrate (called settings I and II by Rhodes and Klug). They are easily distinguished. For example, the 20-bp duplex would have three high points in setting I and two high points in setting II.

Fig. 3 shows a selection of experimental images culled from different runs with different tips so that the common features may be determined. Molecular models are shown (to scale) on the far right. The single-stranded polymers are modeled with a B-like helix with a rise-per-base of 0.33 nm and a twist of 40.5°. They are shown in the azimuthal setting I. The double-stranded polymers are modeled with B-helices with a rise-per-base of 0.33 nm and a twist of 36°. They are shown in azimuthal setting II. We calculated the corresponding images by using the model outlined above. We chose a height of 0.2 nm (consistent with the measurements listed in Table 1) and a Gaussian blurring radius of 0.7 nm (consistent with the known dimensions of our tips). There are no other adjustable parameters. The calculated images are shown next to the experimental images. The agreement is rather good. If our model is correct, it would explain why the sticky ends of sample 4 do not appear in the images. It would also explain why the groove direction is not easy to determine from the images.

Conclusions. We have shown that electrochemical deposition and *in situ* potential control during imaging can be used to obtain reproducible STM images of ssDNA and dsDNA. The images are stable under repeated scanning and show reproducible evidence of internal structure. Features in the images correspond qualitatively to turns of double- and single-stranded helices. A simple tunneling model for contrast produces good agreement with the images if the helices are B-like with a rise-per-base of 0.33 nm and a twist of 40° (single strands) or 36° (duplexes).

We thank Michael Hogan for valuable suggestions. This work was supported by Grant N00014-90-J-1455 from the Office of Naval Research and Grant Dir 89-20053 from the National Science Foundation to S.M.L., Hatch Grant 126 from the Nevada Agricultural Experiment Station, Grant MCB 9117488 from the National Science Foundation, and Grants R01 GM33435 and R55 HG00656 from the National Institutes of Health to R.E.H.; and Grant CA21111 from the National Institutes of Health to A.M.J.

1. Sonnenfeld, R. & Hansma, P. K. (1986) *Science* **232**, 211–213.
2. Lindsay, S. M. (1993) in *Scanning Tunneling Microscopy: Theory, Techniques and Applications*, ed. Bonnell, D. (VCH, New York), pp. 335–408.
3. Beebe, T. P., Wilson, T. E., Ogletree, D. F., Katz, J. E., Balhorn, R., Salmeron, M. B. & Siekhaus, W. J. (1989) *Science* **243**, 370–372.
4. Driscoll, R. J., Youngquist, M. G. & Baldeschweiler, J. D. (1990) *Nature (London)* **346**, 294–296.
5. Clemmer, C. R. & Beebe, T. P. (1991) *Science* **251**, 640–642.
6. Heckl, W. M. & Binnig, G. (1992) *Ultramicroscopy* **42/44**, 1073–1078.
7. Dunlap, D. D., Garcia, R., Schabtach, E. & Bustamante, C. (1993) *Proc. Natl. Acad. Sci. USA* **90**, 7652–7655.
8. Allison, D. P., Bottomley, L. A., Thundat, T., Brown, G. M., Woychick, R. P., Schrick, J. J., Jacobson, K. B. & Wharmack, R. J. (1992) *Proc. Natl. Acad. Sci. USA* **89**, 10129–10133.
9. Lindsay, S. M. & Barris, B. (1988) *J. Vac. Sci. Tech.* **A 6**, 544–547.
10. Lindsay, S. M., Thundat, T., Nagahara, L. A., Knipping, U. & Rill, R. L. (1989) *Science* **244**, 1063–1064.
11. Tao, N. J., DeRose, J. A., Oden, P. I. & Lindsay, S. M. (1991) in *Proceedings of the 49th Annual Meeting of the Electron Microscopy Society of America*, ed. Bailey, G. W. (San Francisco Press, San Francisco), pp. 376–377.
12. Lindsay, S. M., Tao, N. J., DeRose, J. A., Oden, P. I., Lyubchenko, Y. L., Harrington, R. E. & Shlyakhtenko, L. (1992) *Biophys. J.* **61**, 1570–1584.
13. Jing, T., Jeffrey, A. M., DeRose, J. A., Lyubchenko, Y. L., Shlyakhtenko, L. S., Harrington, R. E., Appella, E., Larsen, J., Vaught, A., Rekesh, D. & Lindsay, S. M. (1993) in *Proceedings of the North Atlantic Treaty Organization Advanced Study Institute on Nanoscale Probes of the Solid/Liquid Interface*, eds. Siegenthaler, H. & Gewirth, A. A., in press.
14. Nagahara, L. A., Thundat, T. & Lindsay, S. M. (1989) *Rev. Sci. Instrum.* **60**, 3128–3130.
15. DeRose, J. A., Lampner, D. B. & Lindsay, S. M. (1993) *J. Vac. Sci. Technol.* **A11**, 776–780.
16. Barth, J. V., Brune, H., Ertl, G. & Behm, R. J. (1990) *Phys. Rev. B* **42**, 9307–9318.
17. Gao, X., Hamelin, A. & Weaver, M. (1991) *J. Chem. Phys.* **95**, 6993–6996.
18. Tao, N. J. & Lindsay, S. M. (1991) *Appl. Phy.* **70**, 5141–5143.
19. Tao, N. J. & Lindsay, S. M. (1992) *Surf. Sci. Lett.* **274**, L546–L553.
20. Gupta, G., Garcia, A. E. & Hiriyana, K. T. (1993) *Biochemistry* **32**, 948–960.
21. Gulik, A., Inoue, H. & Luzzati, V. (1970) *J. Mol. Biol.* **53**, 221–238.
22. Saenger, W. (1984) *Principles of Nucleic Acid Structure* (Springer, New York).
23. Tao, N. J., DeRose, J. A. & Lindsay, S. M. (1993) *J. Phys. Chem.* **97**, 910–919.
24. Foster, J. S. & Frommer, J. E. (1988) *Nature (London)* **333**, 542–545.
25. Joachim, C. & Sautet, P. (1989) in *Scanning Tunneling Microscopy and Related Methods*, ed. Behm, R. J. (Kluwer, Dordrecht, The Netherlands), pp. 377–389.
26. Lindsay, S. M., Sankey, O. F., Li, Y. & Herbst, C. (1990) *J. Phys. Chem.* **94**, 4655–4660.
27. Tang, S. L., McGhie, A. J. & Suna, A. (1993) *Phys. Rev. B* **47**, 3850–3856.
28. Yuan, J.-Y., Shao, Z. & Gao, C. (1991) *Phys. Rev. Lett.* **67**, 863–866.
29. Mizutani, W., Shigeno, M., Ohmi, M., Suginoya, M., Kajimura, K. & Ono, M. (1991) *J. Vac. Sci. Technol.* **B 9**, 1102–1105.
30. Jing, T. W., Par, J. & Lindsay, S. M. (1993) in *Proceedings of the North Atlantic Treaty Organization Advanced Study Institute on Nanoscale Probes of the Solid/Liquid Interface*, eds. Siegenthaler, H. & Gewirth, A. A., in press.
31. Schmickler, W. & Henderson, D. (1990) *J. Electroanal. Chem.* **290**, 283–291.
32. Porter, J. D. & Zinn, A. S. (1993) *J. Phys. Chem.* **97**, 1190–1203.
33. Rhodes, D. & Klug, A. (1980) *Nature (London)* **286**, 573–578.
34. Chen, C. J. (1993) *Introduction to Scanning Tunneling Microscopy* (Oxford Univ. Press, New York).
35. Eigler, D. M., Weiss, P. S., Schweizer, E. K. & Lang, N. D. (1991) *Phys. Rev. Lett.* **66**, 1189–1192.
36. Fisher, A. J. & Blöchl, P. E. (1993) *Phys. Rev. Lett.* **70**, 3263–3266.
37. Lang, N. D. (1987) *Phys. Rev. B* **36**, 8173–8176.
38. Büttiker, Imry, Y., Landauer, R. & Pinhas, S. (1985) *Phys. Rev. B* **31**, 6207–6215.
39. Ashcroft, N. W. & Mermin, N. D. (1976) *Solid State Physics* (Holt, Rinehart and Winston, New York).